International Journal of Nanomedicine

Dovepress
open access to scientific and medical research

Open Access Full Text Article

ORIGINAL RESEARCH

Fabrication of multifunctional triple-responsive platform based on CuS-capped periodic mesoporous organosilica nanoparticles for chemo-photothermal therapy

This article was published in the following Dove Press journal:
International Journal of Nanomedicine

Xiangyang Cheng[1,*]
Dejian Li[2,*]
Aiqi Lin[3]
Jun Xu[1]
Liang Wu[1]
Huijie Gu[1]
Zhongyue Huang[1]
Jiangyi Liu[1]
Yiming Zhang[1]
Xiaofan Yin[1]

[1]Department of Orthopedics, Minhang Branch, Zhongshan Hospital, Fudan University, Shanghai 201199, China; [2]Department of Orthopedics, Shanghai Pudong Hospital, Fudan University Pudong Medical Center, Shanghai 201301, China; [3]Department of Retired, Minhang Branch, Zhongshan Hospital, Fudan University, Shanghai 201199, China

*These authors contributed equally to this work

Introduction: For an ideal drug delivery system, the outstanding drug-loading capacity and specific control of the release of therapeutics at the desired lesions are crucial. In this work, we developed a triple-responsive nanoplatform based on copper sulfide (CuS)-capped yolk–shell-structured periodic mesoporous organosilica nanoparticles (YSPMOs) for synergetic chemo-photothermal therapy.

Methods: Herein, the YSPMOs were employed as a drug carrier, which exhibited a high doxorubicin (DOX) loading capacity of 386 mg/g. In this controlled-release drug delivery system, CuS serves as a gatekeeper to modify YSPMOs with reduction-cleavable disulfide bond (YSPMOs@CuS). CuS could not only avoid premature leakage in the delivery process, but also endowed the excellent photothermal therapy (PTT) ability.

Results: Upon entering into cancer cells, the CuS gatekeeper was opened with the breaking of disulfide bonds and the DOX release from YSPMOs(DOX)@CuS in response to the intracellular acidic environment and external laser irradiation. Such a precise control over drug release, combined with the photothermal effect of CuS nanoparticles, is possessed by synergistic chemo-photothermal therapy for cancer treatment. Both in vitro and in vivo experimental data indicated that the synergistic effect of YSPMOs(DOX)@CuS showed efficient antitumor effect. In addition, low systemic toxicity was observed in the pathologic examinations of liver, spleen, lungs, and kidneys.

Conclusion: This versatile nanoplatform combination of PTT, chemotherapeutics, and gating components shows general potential for designing multifunctional drug delivery systems.

Keywords: periodic mesoporous organosilica, CuS, triple-responsive release, chemo-photothermal therapy

Introduction

Cancer is currently one of the most lethal diseases and most severe global health issues.[1] As the pathogenesis of tumor is constantly being recognized, a variety of approaches have been developed for the treatment of cancers.[2–4] Among them, chemotherapy is a predominant approach for the treatment of cancers in the clinic, but it usually causes intense side effects because of the nonspecific biodistribution of anticancer drugs.[5,6] Addressing this arduous challenge is critical to successful treatment. In the past two decades, nanotechnology has brought about a paradigm shift in cancer therapy, and diverse classes of nanoparticle (NP)-based drug delivery have been developed for enhancement of therapeutic efficacy and minimizing the side effects of drugs.

Correspondence: Xiaofan Yin
Department of Orthopedics, Minhang Branch, Zhongshan Hospital, Fudan University, 170 Xinsong Road, Minhang District, Shanghai 201199, China
Tel +86 21 3329 0999
Fax +86 21 3329 0999
Email yxf9029@163.com

submit your manuscript | www.dovepress.com
Dovepress
http://dx.doi.org/10.2147/IJN.S167407

Designing multifunctional drug delivery systems, which specifically control the drug release at the desired sites and are able to deliver combination therapy for more effective cancer treatment, has thus received considerable attention in the area of nanomedicine.[7] Among the reported drug delivery systems, mesoporous silica nanoparticles (MSNs) have emerged as a versatile nanocarrier because of their remarkable biocompatibility and stability, high specific surface area, and, in particular, the controllable drug release behavior.[8–10] Periodic mesoporous organosilica nanoparticles (PMOs), a new kind of MSNs with organic group-incorporated frameworks, represent one of the most exciting achievements in the field of mesoporous materials.[11–13] PMOs have been reported as potential drug carriers because of the controllable size, which is suited to their biologic interactions such as the cellular uptake, blood circulation, tumor accumulation, and so on.[14] It should be noted that the high concentration of organic functional groups in the PMO greatly modifies the biodegradability of NPs, which is crucial for the clinical transformation of biomaterials.[15]

Similar to the MSN-based drug delivery system, controlled gatekeepers capping the pore entrances of PMOs were crucial for achieving specific drug release and avoiding premature leakage in the delivery process before the target site is reached.[16–18] What is more, perfect gatekeepers can only be removed upon exposure to specific internal or external stimuli, thus resulting in the release of the entrapped drugs. A number of capping agents, such as inorganic NPs,[19] organic molecules,[20] peptides,[21] and supramolecular assemblies,[22] have been employed as the responsive "gatekeepers" to fabricate the MSN-based drug delivery systems. Due to the excellent photothermal properties, some inorganic materials serve as a heating gatekeeper coated on MSNs that causes the synergistic effect of tumor cells through combination of chemotherapy and photothermal therapy (PTT), which seems to be an interesting strategy.[23–25] Wang et al first used graphene nanosheet gatekeeper to cap the pore entrances of doxorubicin (DOX)-loaded MSNs.[26] DOX was loaded on the pore wall of targeting peptide-modified MSNs through strong electrostatic interaction, and then the MSNs were capped with graphene. Also, a few PMO drug delivery systems have been reported.[27–29] However, gated PMO drug delivery systems to specifically control the release of therapeutics are still lacking.

Copper sulfide (CuS) NPs have been widely employed as photothermal conversion agents owing to their excellent photothermal conversion property.[30] Moreover, CuS NPs have been demonstrated to have a low long-term toxicity and high biodegradability.[31] A recent study by Su et al reported CuS as a gatekeeper to cap the mesoporous upconversion NPs, which fabricated a multifunctional mesoporous upconversion NP-based drug controlled-release system for upconversion luminescence emission/magnetic resonance imaging/photoacoustic tomography-guided synergetic chemo-thermotherapy.[32] However, to the best of our knowledge, there is no report on gating of the CuS with PMO NPs for tumor treatment.

Herein, we present a facile CuS-gated PMO triple-responsive nanoplatform. The PMO was employed as the carrier to encapsulate chemotherapeutic agent DOX. The linker cysteamine was used to introduce the cleavable disulfide bonds (-SS-) and conjugate the gatekeeper L-cysteine-CuS (CuS-Lys) to the pore entrance, which can prevent drug burst release during the delivery. It is also an excellent photothermal agent and is used for photothermal ablation therapy. Once the yolk–shell periodic mesoporous organosilica nanoparticles or yolk–shell PMOs (YSPMOs(DOX)@CuS) is taken up by the cancer cells, the breaking of disulfide linkers is triggered by the high concentration of glutathione (GSH) in cancer cells, and thus the resulting CuS capping agent on the surface of YSPMOs can be removed leading to rapid drug release in the cytoplasm. Meanwhile, CuS can be used to precisely generate hyperthermia in tumor sites upon light irradiation. We carried out synergistic chemo-photothermal therapy for in vitro and in vivo sarcomaia 180 (S180) tumor. The results demonstrated that the triple-responsive nanoplatform significantly inhibits tumor growth, suggesting its great potential for synergistic therapy of cancer (Figure 1).

Experimental

Materials

Tetraethoxysilane (TEOS), cetyltrimethyl ammonium bromide (CTAB), concentrated ammonia (25 wt%), copper chloride ($CuCl_2$), sodium sulfide (Na_2S), GSH, L-cysteine, and anhydrous ethanol were purchased from Sinopharm Chemical Reagent Co., Ltd (Shanghai, China). The 3-mercaptopropyltrimethoxysilane (MPTMS), DOX hydrochloride, and 1,4-bis-(triethoxysilyl) propane tetrasulfide (TESPTS) were obtained from Sigma-Aldrich (St Louis, MO, USA). Cysteamine, N-[3-(dimethylamino)propyl]-N′-ethylcarbodiimide hydrochloride (EDC), N-hydroxysuccinimide (NHS), and fluorescein isothiocyanate were purchased from Aladdin Reagent (Shanghai, China). Deionized (DI) water (H_2O) used in all experiments was purified by a Millipore system (Milli-Q, 18.2 MΩ cm). Dimethyl sulfoxide (DMSO), fetal bovine serum (FBS), PBS, antibiotics (penicillin/streptomycin), and DMEM were supplied by the Shanghai

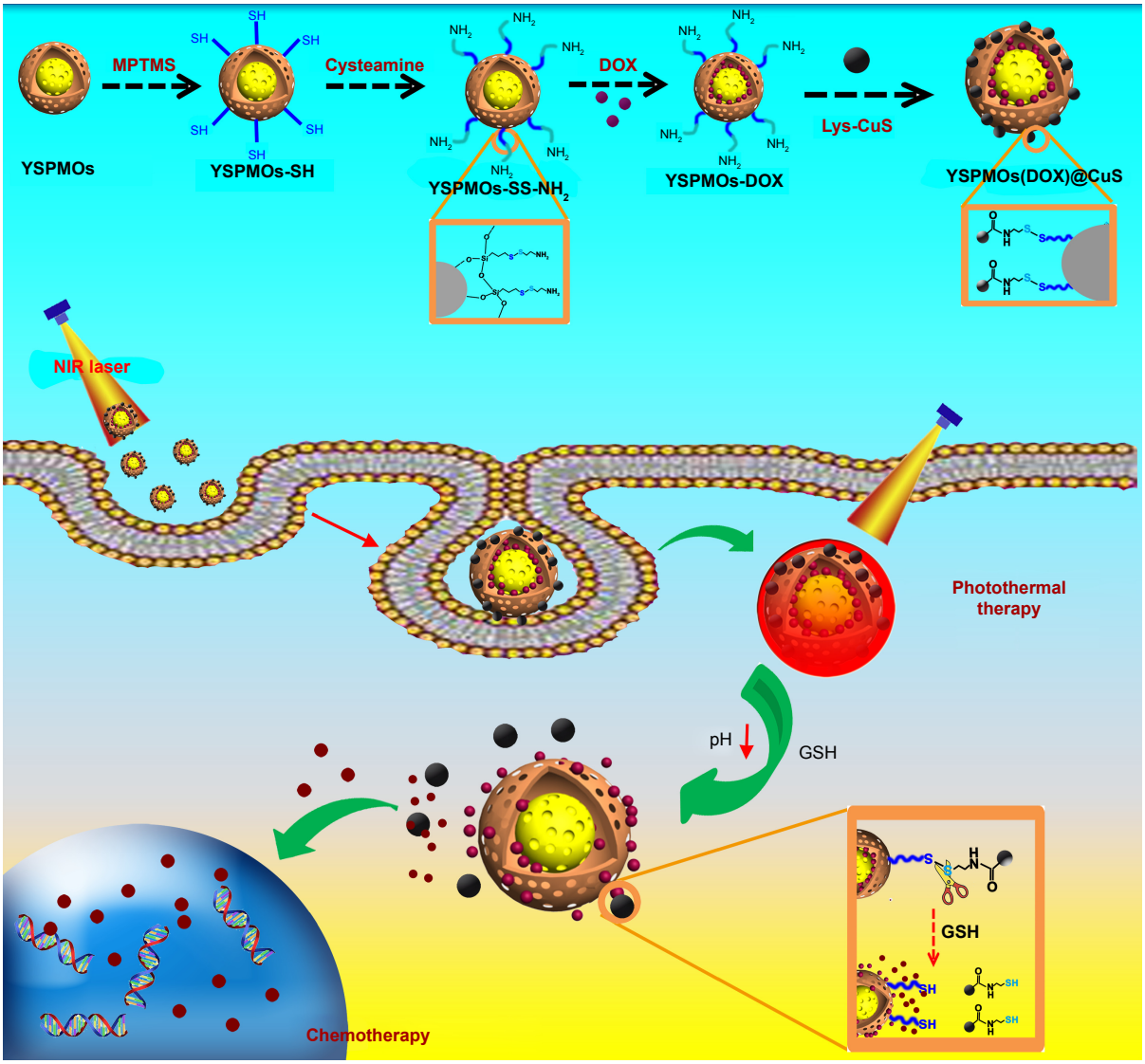

Figure 1 Schematic illustration of the preparation processes of multifunctional triple-responsive platforms for chemo-photothermal therapy.
Abbreviations: DOX, doxorubicin; GSH, glutathione; Lys, L-cysteine; MPTMS, 3-mercaptopropyltrimethoxysilane; YSPMOs, yolk–shell-structured periodic mesoporous organosilica nanoparticles.

Pumai Biotechnology Co. Ltd. MTT and 4-6-diamidino-2-phenylindole (DAPI) were purchased from Nanjing KeyGen Biotech. Co. Ltd (Nanjing, China). The human cancer MDA-MB-231 cell lines and S180 cell lines were provided by the Institute of Biochemistry and Cell Biology, Chinese Academy of Sciences (Shanghai, China).

Preparation of YSPMOs-SH

Thioether-bridged YSPMOs were first synthesized according to a sol–gel method in the literature, with some modification.[15,33] In a typical synthesis, CTAB (0.2 g) was added into a mixture of concentrated aqueous ammonia solution (1.25 mL, 25 wt%), n-propanol (30 mL), and water (180 mL), and then stirred for 30 min to form a clear solution at 35°C in an oil bath. Then, a mixture of TEOS (0.34 mL) and TESPTS (0.18 mL) was quickly injected into the above solution. After stirring at 35°C for 24 h, the white product was collected by centrifugation at 10,000 rpm for 10 min, and washed three times with ethanol. To obtain the YSPMOs, the solid product was dispersed in 40 mL of water and transferred to a teflon-lined stainless-steel autoclave and heated at 150°C for 24 h. Afterwards, the reaction solution was cooled down to room temperature and the solid product was dispersed in 60 mL of ethanol containing 120 µL of HCl and stirred at 60°C for 3 h with reflux condensation. The extraction was repeated three times to remove the CTAB template. Finally, the sample was dried in vacuum to yield the YSPMOs. Next, the YSPMOs (150 mg) were dispersed in ethanol (150 mL),

into which 1.5 mL of MPTMS and 0.2 mL of ammonia solution were added. The mixture was stirred overnight and the YSPMOs-SH was collected by centrifugation and washed three times with ethanol.

Preparation of YSPMOs-SS-NH_2

To prepare disulfide linkage-modified YSPMOs, 100 mg YSPMOs-SH was dispersed in 50 mL DI water, and then 200 mg cysteamine dissolved in 10 mL DI water was added. After stirring for 24 h, the YSPMOs-SS-NH_2 was obtained by dialysis against DI water for 1 day, and thn drying the NPs under vacuum.

Synthesis of Lys-CuS NPs

The Lys-CuS NPs were prepared according to the previous study.[32] In 150 mL of DI water, 0.12 mM of L-cysteine was dissolved. $CuCl_2$ solution (50 mL, 25 mM) was then added to the solution under vigorous stirring. The pH of the solution was adjusted to 3.0 with hydrogen nitrate solution after stirring for 30 min. Then, 15 mL of Na_2S aqueous solution was added under stirring at 90°C for 1.5 h and then the system was transferred into an ice bath to stop the reaction. The synthesized product was harvested and purified by centrifugation. Finally, the Lys-CuS NPs were dispersed in DI water for later use.

Synthesis of YSPMOs(DOX)@CuS

DOX was chosen as the model drug. Drug loading was carried out by soaking YSPMOs-SS-NH_2 (100 mg) in 50 mL DI water containing 50 mg DOX, at pH 7.4 and room temperature, for 24 h in the dark. The DOX-loaded NPs were referred to as YSPMOs(DOX). Meanwhile, the loading capacity was evaluated according to the changes in DOX concentration before and after loading. For CuS capping, 50 mg of Lys-CuS was dispersed in pH 7.4 PBS containing EDC (23.0 mg, 0.12 mmol) and NHS (13.8 mg, 0.12 mmol) to activate the carboxyl group. After being stirred for 2 h, 50 mg of YSPMOs(DOX) was added to the above solution. The solution was stirred at room temperature for 24 h. After centrifugation and washing with water several times, the DOX-loaded and CuS-gated NPs were designated as YSPMOs(DOX)@CuS. Meanwhile, the preparation of YSPMOs@CuS NPs was the same without the DOX loading.

Characterization

Transmission electron microscopy (TEM) imaging and energy-dispersive spectroscopy of these NPs were performed on an FEI Tecnai F20 instrument with an acceleration voltage of 200 kV. The size and zeta potential of the materials were measured with a Malvern Zetasizer Nano ZS instrument (Malvern Instruments, Malvern, UK). X-ray diffraction (XRD) measurements were performed on a D/Max-2550 PC X-ray diffractometer equipped with graphite-monochromatized Cu Kα radiation (Rigaku, Geigerflex D/Mac, Japan). N_2 adsorption/desorption isotherms were obtained by an absorption analyzer ASAP 2020, Micromeritics, New York, USA and the specific surface area and pore size were obtained by Brunauer–Emmett–Teller and Barrett–Joyner–Halenda methods, respectively. Fourier transform infrared (FT-IR) spectra were recorded on a Nicolet iS10 spectrometer (Thermo Fisher Scientific, MA, USA). UV–Vis absorption spectra were recorded on a UV-1800 spectrophotometer (Shanghai JingHua Instruments). The content of copper ions in the solution was determined by inductively coupled plasma-optical emission spectroscopy (ICP-OES, Hudson, New York, USA). The photothermal conversion efficiency of the materials was analyzed using a 980 nm laser device (STL808T1-7.0 W, STL808T1-7.0 W, Beijing STONE Laser, Beijing, China) and the temperature of the solution was monitored using a DT-8891E thermocouple linked to a digital thermometer (Shenzhen Everbest Machinery Industry, Shenzhen, China).

Photothermal performance of YSPMOs@CuS

To determine the photothermal effect of YSPMOs@CuS, 200 μL of different concentrations of YSPMOs@CuS in PBS were put in 0.25 mL eppendorf tubes, which were subjected to a 980 nm near infrared (NIR) laser for 3 min with different laser powers. The temperature changes of the solutions were recorded by thermocouple thermometer. Meanwhile, the changes in temperature were measured using YSPMOs and PBS as control groups under the same conditions. Finally, the samples were irradiated for 5 min with five on–off cycles to detect the thermal stability of YSPMOs@CuS samples. Moreover, the photothermal conversion efficiency was calculated by the following equation[34]:

$$\eta = \frac{hS\,(T_{max} - T_{am}) - Q_0}{I\,(1 - 10^{-A})}$$

where h is the heat transfer coefficient, S the surface area, T_{max} the equilibrium temperature, T_{am} the surrounding ambient temperature, Q_0 the heat absorption of the quartz cell, I the laser power, and A is the absorbance of the materials at 980 nm.

In vitro triple-responsive drug release

To investigate the triple stimuli (GSH, pH, and NIR laser)-responsive DOX release from the YSPMOs(DOX)@CuS,

0.5 mL YSPMOs(DOX)@CuS (4 mg/mL) was incubated in 2 mL of PBS buffer (pH 7.4 or pH 5.8), with and without the addition of 10 mM GSH and 980 nm NIR laser irradiation, separately, for different periods of time. In the case of laser irradiation, YSPMOs(DOX)@CuS nanocomposite samples were additionally irradiated by a 980 nm NIR laser (1.0 W/cm^2) for 5 min every hour. At predetermined time intervals, the sample solutions (1 mL) were taken out from the solution for analysis, and equivalent fresh PBS solutions were supplemented. DOX release was determined by measuring the absorption intensity at 480 nm by UV–Vis spectrometer.

In vitro cytotoxicity assay

The human cancer MDA-MB-231 cells were incubated in DMEM supplemented with 10% (v/v) FBS, 1% (v/v) penicillin, and 1% (v/v) streptomycin. Cells were cultured in a humidified incubator at 37°C with 5% CO_2. The cytotoxicity of YSPMOs@CuS or YSPMOs(DOX)@CuS was measured by MTT assay. The MDA-MB-231 cells were seeded at 5×10^3 cells per well in 96-well plates and cultured for 24 h. Then culture medium was replaced by DMEM containing various concentrations of YSPMOs(DOX)@CuS or YSPMOs@CuS and free DOX. For the laser irradiation group, cells were immediately irradiated by 980 nm laser of 1.0 W/cm^2 for 10 min. Untreated cells in growth media were used as the blank control. Then, the cells were washed with PBS and incubated for 24 h. Subsequently, 20 μL of MTT was added and the plates were incubated for another 4 h at 37°C in the dark. Afterwards, the medium was removed and 100 μL of DMSO was added to dissolve the blue formazan crystals. The absorbance of the formazan was detected with a microplate reader (BioTek, Winooski, VT, USA) at 570 nm to determine the relative cell viability of the different groups.

In vitro cellular uptake assay

Cellular uptake experiments of YSPMOs(DOX)@CuS against MDA-MB-231 cells were performed by using confocal laser scanning microscopy (CLSM, Nikon C1-si, Tokyo, Japan) and a flow cytometer (FC500, Beckman, California, USA). MDA-MB-231 cells were seeded in six-well plates at a density of 5×10^4 cells per well and cultured for 24 h. Then, the medium was removed and replaced with 2 mL of fresh medium containing YSPMOs(DOX)@CuS or free DOX at a DOX concentration of 5 μg mL^{-1} for 4 h followed by washing the cells with PBS. Thereafter, the cells of the photothermal group were illuminated (980 nm, 1 W/cm^2) for 10 min. After another 2 h incubation, the cells were washed three times with PBS and fixed with 4% formaldehyde for 20 min, and again washed with PBS three times. The cell nuclei were stained with DAPI for 10 min. Subsequently, the cells were washed with PBS three times and observed by CLSM. For flow cytometry analysis, the cells were seeded in six-well plates (1×10^5 cells/well). After incubation for 24 h, the medium was replaced with DMEM containing free DOX or YSPMOs(DOX)@CuS with or without laser irradiation. After incubation for another 3 h, the cells were then centrifuged, washed with PBS buffer, resuspended in PBS buffer, and analyzed for fluorescence intensity with a flow cytometer.

Meanwhile, the specific cellular uptake of the YSPMOs (DOX)@CuS within MDA-MB-231 cells was tested by quantitative ICP-OES analysis according to the literature.[35]

In vivo cancer treatment

All animal experimental procedures were undertaken in accordance with the guidelines for the animal experiments, and were performed following a National Institutes of Health Animal Care and Use Committee-approved protocol. Ethical approval for all experiments was obtained from the Animal Care and Use Committee of Fudan University before beginning in vivo work. Male 4- to 6-week-old BALB/c nude mice (15–20 g) were purchased from Shanghai Slac Laboratory Animal Center (Shanghai, China). To induce a solid tumor, murine sarcoma S180 cells (5×10^6 in 100 μL PBS) were injected subcutaneously into the right shoulder of the BALB/c nude mice. Treatments were carried out when the tumors reached 100 mm^3. The mice were observed daily and the tumor sizes were measured by a caliper every 2 days, and the tumor was estimated by the following formula: tumor volume=(tumor length)×(tumor width)^2/2. Relative tumor volumes were calculated as V/V_0 (V_0 was the initial tumor volume).

To assess the therapeutic performance of YSPMOs (DOX)@CuS on solid tumor, the S180 tumor-bearing nude mice were randomly allocated to four groups (n=5): saline control, free DOX, YSPMOs(DOX)@CuS, and YSPMOs(DOX)@CuS plus laser irradiation. One hundred microliters of different formulations (DOX dose: 5 mg kg^{-1}) was administrated through tail vein injection every 2 days. For the PTT group, 980 nm NIR laser at a density of 1 W/cm^2 was applied to irradiate the tumor site for 10 min at 2 h after injection. The tumor volume was measured every 2 days. After treatment, the main tissues (heart, liver, spleen, lung, and kidney) and tumors from the four groups were collected, and fixed in paraformaldehyde, embedded in paraffin, sectioned, and stained with hematoxylin and eosin (H&E), and subsequently examined by BX41 bright field microscopy (Olympus, Tokyo, Japan).

In vivo biodistribution

S180 tumor-bearing mice (three mice for each group) were intravenously injected with YSPMOs(DOX)@CuS at the same dose as for in vivo cancer therapy. At different time intervals post-injection (6, 12, and 24 h), the mice were euthanized and the major organs (heart, liver, spleen, lung, and kidney) and tumor were collected, lyophilized, weighed, and digested by aqua fortis for ICP-OES measurement to determine the content of Cu element in the organs.

Statistical analysis

Data are expressed as mean±SD. Student's *t*-test statistical analysis was performed with SPSS 16.0 software, and the criterion for statistical significance was $*p<0.05$ and $**p<0.01$.

Results and discussion

Synthesis and characterization of YSPMOs(DOX)@CuS NPs

The multifunctional triple-responsive drug-delivery system incorporating chemotherapy and PTT into a nanoplatform is schematically illustrated in Figure 1. YSPMOs with thioether-bridged yolk–shell structure were first synthesized according to a sol–gel method followed by hydrothermal treatment.[33] To modify the YSPMOs, thiol functional groups were introduced onto the pore outlet. Then, the thiol-functionalized YSPMOs (YSPMOs-SH) were treated with cysteamine to achieve YSPMOs-SS-NH_2 with disulfide bond, which could be broken by a relatively high level of GSH in tumor cells. The NPs were first characterized by TEM (Figure 2A). Figure 2B reveals that the obtained CuS-Lys NPs had an average diameter of 6.5 nm. Several diffraction rings were observed in the typical selected area electron diffraction pattern of CuS-Lys NPs (Figure 2C), which demonstrated that the NPs had a good crystal structure.[36] The TEM image showed that CuS-Lys NPs could be firmly attached on the surface of the YSPMO nanospheres (Figure 2D) and they did not alter the overall morphology. The coexistence of Cu and S elements was observed in the energy-dispersive spectra of YSPMOs(DOX)@CuS (Figure S1), within which Si and O elements derived from YSPMOs were presented, indicating the successful CuS conjugation. It can be seen

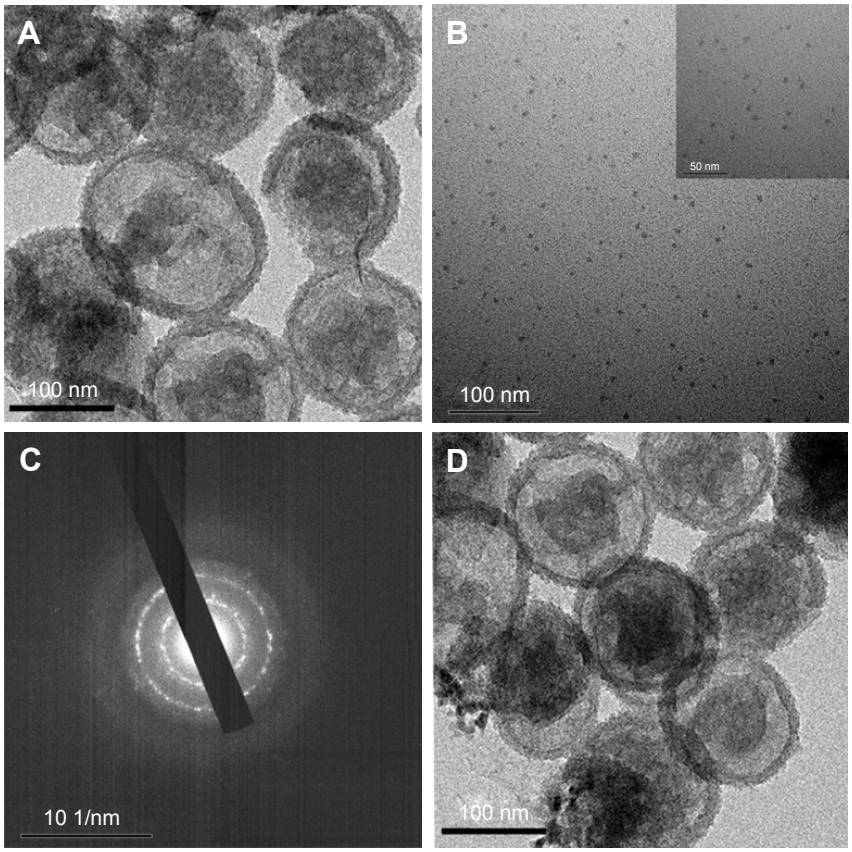

Figure 2 Characterization of the nanoparticles.
Notes: TEM images of the as-made YSPMOs-SH (**A**) and CuS-Lys NPs (**B**). (**C**) SAED pattern of CuS NPs. (**D**) TEM images of YSPMOs(DOX)@CuS NPs.
Abbreviations: DOX, doxorubicin; Lys, L-cysteine; SAED, selected area electron diffraction; TEM, transmission electron microscopy; YSPMOs, yolk–shell-structured periodic mesoporous organosilica nanoparticles.

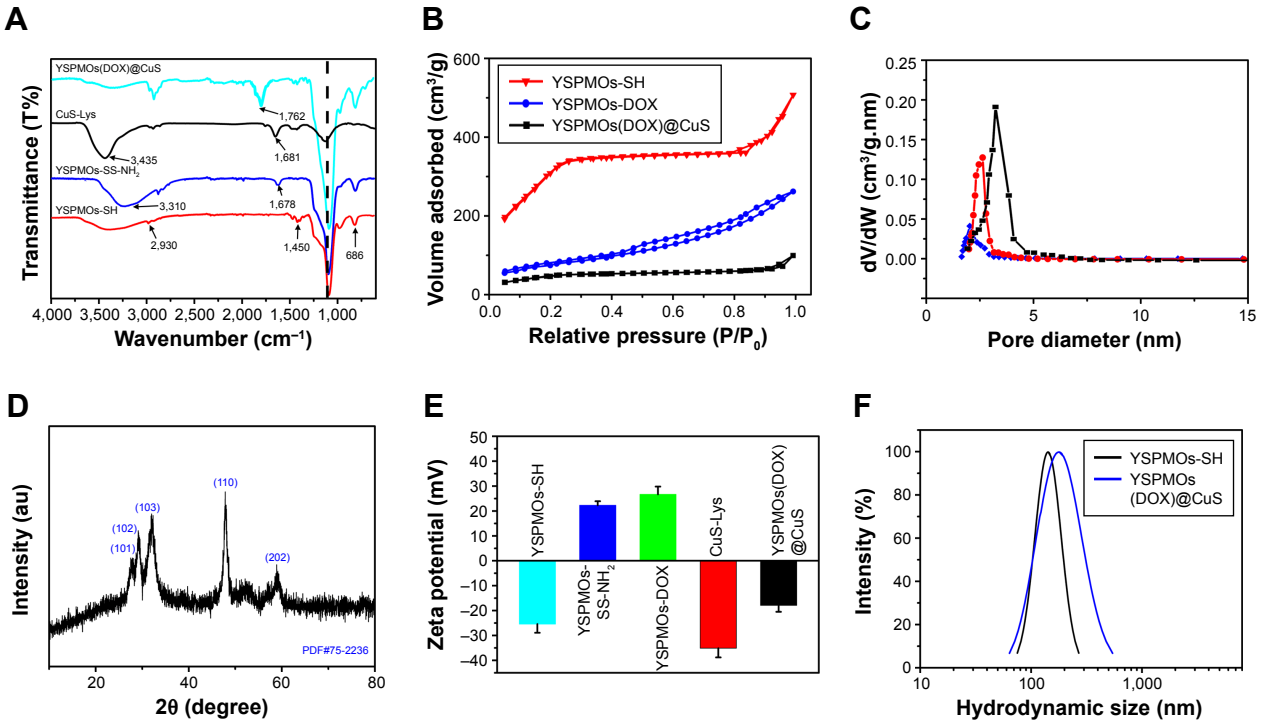

Figure 3 Physicochemical properties of YSPMOs(DOX)@CuS NPs.

Notes: (**A**) FT-IR spectra of different functionalized YSPMOs. (**B**) Nitrogen adsorption–desorption isotherm and (**C**) the pore size distribution of different YSPMOs. (**D**) XRD data of the as-prepared CuS-Lys NPs. (**E**) The surface charge potentials of different functionalized YSPMOs. (**F**) DLS measurement of the size distribution of YSPMOs-SH and YSPMOs(DOX)@CuS.

Abbreviations: DLS, dynamic light scattering; DOX, doxorubicin; FT-IR, Fourier transform infrared; Lys, L-cysteine; XRD, X-ray diffraction; YSPMOs, yolk–shell-structured periodic mesoporous organosilica nanoparticles.

that the YSPMOs display a diameter of about 150 nm with a yolk−shell structure. Also, FT-IR spectrum of the PMOs shows C–H bands at 2,930 and 1,450 cm^{-1} and C–S band at 686 cm^{-1}, demonstrating the thioether-bridged frameworks[37] (Figure 3A). After being modified with cysteamine, the presence of a typical NH_2 stretching vibration of cysteamine at 1,678 cm^{-1} was observed in the spectrum of YSPMOs-SS-NH_2, which confirmed the appearance of amino groups on the silica NPs. The variation of surface area and average pore size during the process of modification was also monitored by N_2 adsorption–desorption isotherms and the results indicated that YSPMOs-SS-NH_2 exhibited a slight decrease in specific surface area (684 m^2 g^{-1}) and uniform pore size of 2.67 nm as compared to original YSPMOs (Figure 3B and C). But this is enough to make YSPMOs-SS-NH_2 suitable for drug delivery. Certainly, the anticancer drug DOX can be successfully loaded into the mesoporous channel of YSPMOs-SS-NH_2.

Meanwhile, XRD pattern shows that the crystal structure of CuS-Lys belongs to the covellite phase with the existence of strong characteristic (101), (102), (103), (110), and (202) peaks (Figure 3D).[38,39] After the resultant YSPMOs-SS-NH_2 NPs were loaded with DOX, the CuS NPs as the "gatekeeper" capped on pore outlets through the formation of an amide covalent bond between L-cysteine and YSPMOs-SS-NH_2, finally resulting in CuS-gated NPs (YSPMOs(DOX)@CuS). FT-IR spectrum of YSPMOs(DOX)@CuS showed a band of amide at around 1,762 cm^{-1} (Figure 3A), which further confirmed that the CuS-Lys NPs were successfully conjugated on the YSPMOs-DOX. Afterwards, the introduction of the gatekeeper CuS was confirmed by the variations of zeta potential from +26.7 to −17.9 mV (Figure 3E). Meanwhile, the content of CuS in YSPMOs(DOX)@CuS was further measured by using ICP analysis, confirming 100 μg of copper per mg of YSPMOs(DOX)@CuS. As expected, the pore size and surface area of YSPMOs-SS-NH_2 decreased dramatically after DOX loading and CuS gating (Figure 3B and C). The DLS results showed that YSPMOs-SH and YSPMOs(DOX)@CuS display narrow size distribution, and the hydrodynamic diameter was increased from 186.7 nm for YSPMOs-SH to 222.6 nm for YSPMOs(DOX)@CuS (Figure 3F). Subsequently, the stability of YSPMOs(DOX)@CuS nanocomposites was investigated through DLS analyses. As shown in Figure S2, the size distributions of YSPMOs(DOX)@CuS in H_2O, PBS, and DMEM demonstrate good stability in different media.

After validating the successful fabrication of multifunctional hybrid YSPMOs, the drug-loading capability of

YSPMOs-SS-NH_2 was measured through UV–Vis spectroscopy to be 89.4% and 158.9 μg DOX per mg of nanocarriers. In addition, YSPMOs-DOX exhibited the typical UV–Vis absorbance peak of DOX at 480 nm (Figure 1F), confirming that DOX had been loaded into the YSPMOs. Also, the UV–Vis absorption spectrum of the YSPMOs(DOX)@CuS presents the absorption peaks of CuS at 1,100 nm, further demonstrating the successful gating of CuS around the PMO–Dox (Figure 4A). Meanwhile, the YSPMOs(DOX)@CuS nanocomposites also display strong absorption in the

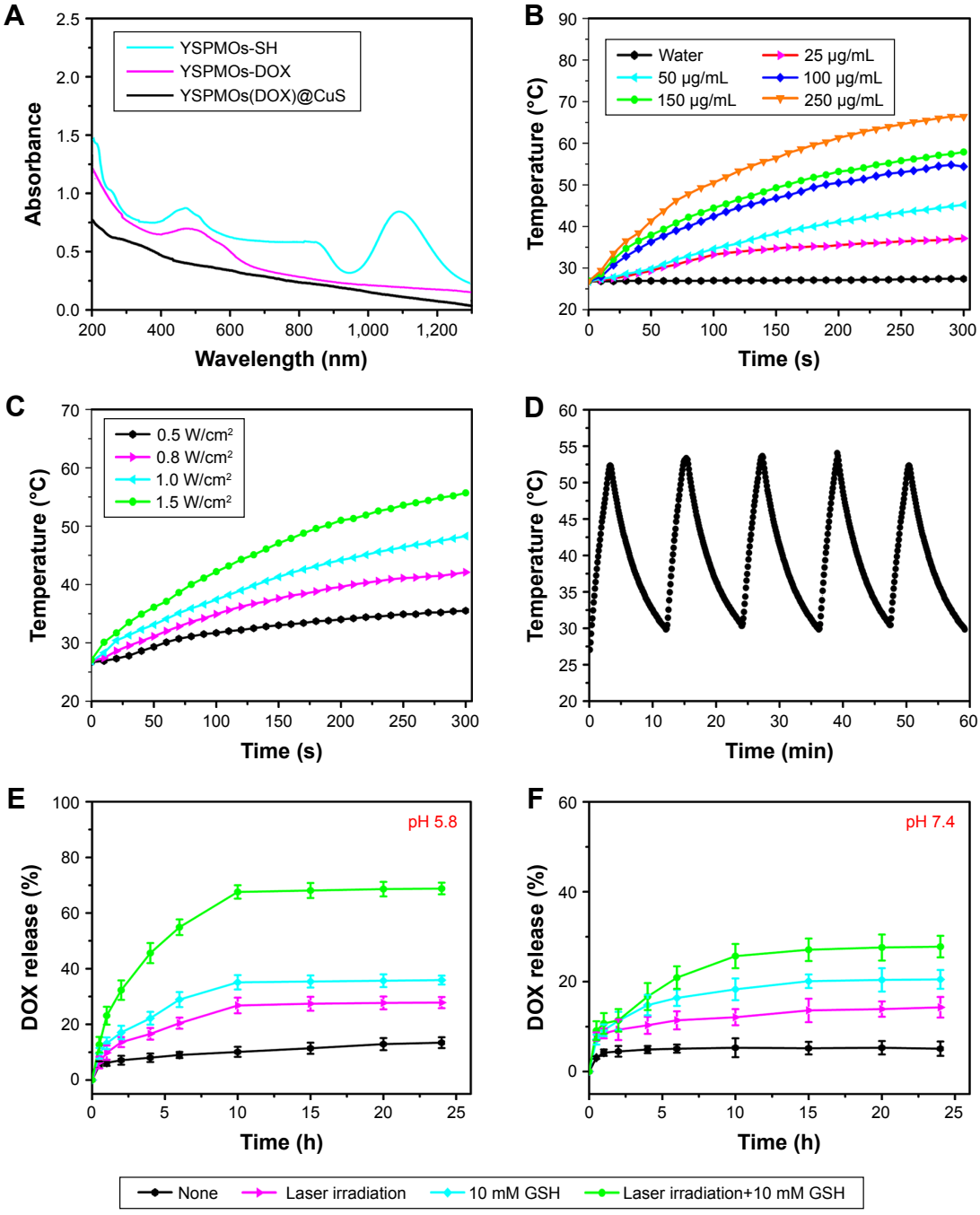

Figure 4 Photothermal properties of YSPMOs(DOX)@CuS NPs and in vitro drug release.

Notes: (**A**) UV–Vis spectra of YSPMOs-SH, YSPMOs-DOX, and YSPMOs(DOX)@CuS. (**B**) Temperature changes of different concentrations of YSPMOs(DOX)@CuS and pure water after 5 min with 980 nm laser irradiation (laser power density: 1.0 W/cm²). (**C**) Temperature changes of YSPMOs(DOX)@CuS solution (50 μg/mL) after 5 min at different power densities of 980 nm laser irradiation. (**D**) Photothermal stability study of YSPMOs(DOX)@CuS. (**E**) Release kinetics of DOX from YSPMOs(DOX)@CuS in the presence and absence of GSH and irradiation in PBS buffer at (**E**) pH=5.8 and (**F**) pH=7.4.

Abbreviations: DOX, doxorubicin; UV–Vis, ultraviolet–visible; YSPMOs, yolk–shell-structured periodic mesoporous organosilica nanoparticles.

NIR region because of the CuS conjugation, suggesting that they can be used as an outstanding photothermal agent.

Photothermal properties of the YSPMOs@CuS NPs

Inspired by the effective NIR absorbance of CuS NPs, the photothermal effect of CuS-gated YSPMOs was also evaluated. The temperature changes of pure water and YSPMOs@CuS aqueous dispersions with different concentrations were recorded under a 980 nm laser irradiation (1.0 W/cm^2) for 5 min. It can be observed that the temperature of pure water only increased slightly, while the YSPMOs@CuS aqueous dispersions presented a significant increase, and the increases were concentration dependent (Figure 4B). For instance, the temperature of the solution at a concentration of 100 μg mL^{-1} reached 54.4°C, which was high enough to kill cancer cells.[40] The laser power density–dependent temperature increases for YSPMOs@CuS aqueous solutions can be observed from Figure 4C. These results demonstrated that the YSPMOs@CuS could efficiently convert laser energy into heat energy. Meanwhile, YSPMOs@CuS aqueous dispersion show a desirable photothermal stability at least within five cycles of laser irradiation/cooling down (Figure 4D), which is of significance for their PTT applications.

In vitro triple-responsive drug release

The level of intracellular GSH concentration can reach 1−11 mM, which is much higher than that of the extracellular concentration (10 μM), and GSH concentration of tumor cells is quite different from that of normal cells.[6,41] In our design, once the YSPMOs(DOX)@CuS nanocomposites enter the cells, tumor intracellular GSH will cause the cleavage of disulfide bonds, thus resulting in the removal of the CuS gatekeeper from the nanocarrier for the DOX release. To verify the gating effect of CuS NPs, in vitro drug release with varying conditions was carried out. The YSPMOs(DOX)@CuS NPs were explored under PBS (pH 5.8 and pH 7.4) in the presence or absence of GSH (10 mM) and light irradiation, and their release efficiency was evaluated. As expected, YSPMOs(DOX)@CuS showed no obvious release at pH 7.4 and 5.8 without any other stimulus, indicating that CuS could efficiently prevent the drug leakage. In contrast, drug release was dramatically increased when 10 mM GSH was added into the YSPMOs(DOX)@CuS. For example, the release amount of DOX reached 35.1% at the end of 10 h in 10 mM GSH solution, much higher than that without GSH. This finding is due to the GSH-induced cleavage of disulfide bonds and consequent leaving of the blocking CuS on pore outlets, indicating that the stimuli-triggered release of encapsulated DOX could be realized with the assistance of GSH. Furthermore, the effect of NIR laser irradiation on the DOX release was further examined. As shown in Figure 4E and F, pure laser irradiation can only promote drug release to some extent because of the protection of the CuS gatekeeper. However, the release of DOX could be accelerated upon NIR laser irradiation together with GSH, which reached 67.6% in 10 h in this case, especially in acidic environment (Figure 4E). In addition, the rapid DOX release was observed at pH 5.8, which stimulated the intracellular endo/lysosomal environment, reaching 68.8% upon light irradiation in the presence of GSH, which is much higher than that of 27.7% at the same GSH concentration in neutral condition (Figure 4F), indicating a pH-responsive drug release property. The phenomenon can be attributed to the reduction of electrostatic interaction between DOX and YSPMOs.[26] Taking into account that tumor cells exhibit much higher GSH concentration, and are more acidic than normal cells, the GSH/pH/laser triple-responsive platform YSPMOs(DOX)@CuS is a versatile strategy that could achieve on-demand release of anticancer drugs.

In vitro cytotoxicity was then evaluated by MTT assay to demonstrate the potential cytotoxicity of YSPMOs@CuS and the therapeutic efficacy of different formulations. Without loading DOX, YSPMOs@CuS exhibited a negligible toxicity against MDA-MB-231 cells even at a high concentration of 200 μg mL^{-1} (Figure S3), indicating good biocompatibility of the nanocarriers. After loading with DOX, a drug concentration-dependent cell inhibition was observed (Figure 5A). Furthermore, the therapeutic efficacy of YSPMOs(DOX)@CuS upon NIR laser irradiation was evaluated. As expected, cells treated with YSPMOs(DOX)@CuS upon NIR laser irradiation (1.0 W/cm^2, 10 min) showed a higher cell toxicity than the chemotherapy alone (without NIR irradiation) or the PTT alone at all tested concentrations (Figure 5B). Therefore, it is concluded that the YSPMOs(DOX)@CuS nanocomposites act as a multifunctional nanoplatform and could offer an obvious synergistic chemo-photothermal killing effect for cancer cells.

In vitro cellular uptake

It is well known that the efficient internalization of NPs into cells is very important in cancer therapy. Owing to the photothermal conversion property of CuS, the local mild hyperthermia could accelerate cellular uptake of nanocarriers and the light-triggered drug release inside cells under the tumor microenvironment. To verify this, YSPMOs(DOX)@CuS

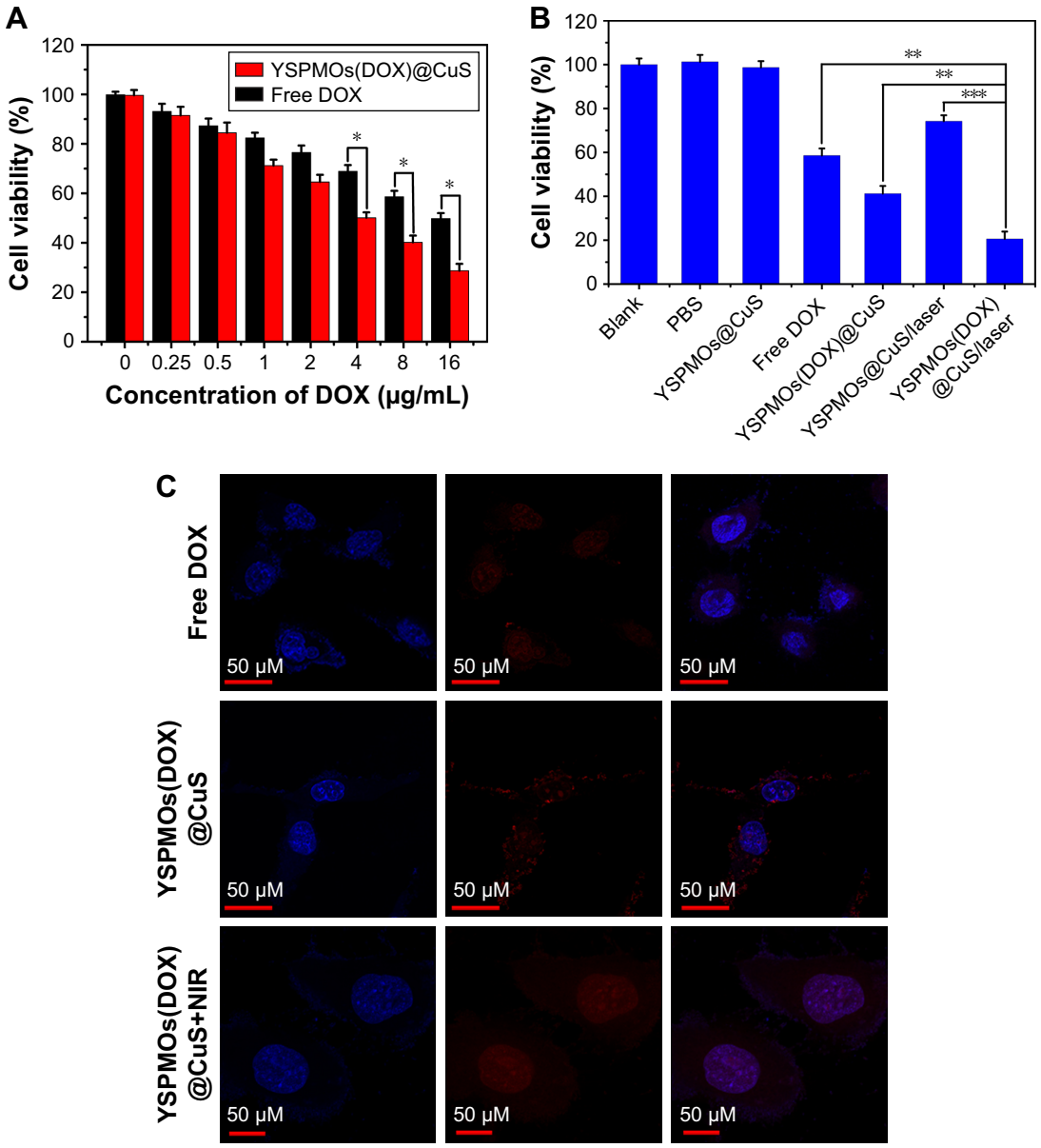

Figure 5 In vitro cell viability and cellular uptake.

Notes: (**A**) Cell viability of MDA-MB-231 cells incubated with different concentrations of DOX and YSPMOs(DOX)@CuS (equivalent concentration of DOX). (**B**) Cell viability of MDA-MB-231 cells treated with different forms of the nanocomposite with or without NIR laser irradiation (980 nm, 1.0 W/cm^2). (**C**) CLSM of MDA-MB-231 cells treated with free DOX and YSPMOs(DOX)@CuS with or without NIR laser irradiation. *P<0.05, **P<0.01, ***P<0.001.

Abbreviations: CLSM, confocal laser scanning microscopy; DOX, doxorubicin; NIR, near infrared; YSPMOs, yolk–shell-structured periodic mesoporous organosilica nanoparticles.

and free DOX were both administered to MDA-MB-231 cells with or without laser irradiation for 10 min. DAPI was used for nuclear localization, and then the fluorescence of DOX in cells was monitored by CLSM. As shown in Figure 5C, without laser irradiation, only a sporadic red fluorescence signal was observed in YSPMOs(DOX)@CuS group because DOX was released in response to intracellular GSH and acidic environment. In contrast, much stronger red fluorescence was observed inside the nuclei after irradiation (980 nm, 1.0 W/cm^2) for 10 min. These results strongly confirm that the NIR laser irradiation can enhance the cell uptake of YSPMOs(DOX)@CuS, thus resulting in the intracellular DOX release. The enhanced cellular uptake of YSPMOs(DOX)@CuS with laser irradiation, mainly because of the local mild hyperthermia induced by laser, could cause cell membrane disruptions to some extent, thus promoting the cellular internalization of the NPs.[42,43] Meanwhile, flow cytometry was used to quantify the red fluorescence signal intensity of DOX. Figure S4 shows that MDA-MB-231 cells treated with YSPMOs(DOX)@CuS and NIR irradiation exhibited stronger fluorescence intensity than those treated with YSPMOs(DOX)@CuS without NIR irradiation and free

DOX, respectively, again demonstrating that the mild hyperthermia facilitated the internalization of YSPMOs(DOX)@CuS and stimulated the DOX release.

In addition, to further verify that the cell uptake of nanocarriers is enhanced by mild hyperthermia, the cellular uptake of the YSPMOs(DOX)@CuS nanocomposites by MDA-MB-231 cells was evaluated by ICP-OES. It can be seen that the Cu uptake in laser irradiation group was 1.3, 1.5, and 1.6 times higher than that in YSPMOs(DOX)@CuS without laser irradiation ($p<0.01$) at particle concentrations of 100, 50, and 25 μg/mL, respectively (Figure S5). These results were consistent with enhanced internalization and accumulation of NPs in cells, especially under laser irradiation.

In vivo antitumor activity

Encouraged by the attractive ability of NIR-triggered enhanced cellular uptake of NPs, and triple-responsive drug release, shown above with DOX-loaded YSPMOs(DOX)@CuS nanocomposites, we tried to utilize this system for in vivo antitumor efficacy. Here, the S180 tumor-bearing nude mice were used to evaluate the antitumor efficacy in vivo of YSPMOs(DOX)@CuS. Formulations were intravenously injected into the mice containing comparable amounts of DOX and the photothermal group followed by NIR irradiation for 10 min at 8 h post-injection and the tumor sizes were periodically monitored. As illustrated in Figure 6A, the tumor of the untreated control group displayed a rapid growth volume, while the groups treated with free DOX presented mild tumor volume inhibition during the assay period. The growth of S180 tumors was slightly inhibited by YSPMOs(DOX)@CuS, but the performance was far from satisfactory because of the lower accumulation of free DOX in the tumor site.[19] In contrast, the tumors treated with the YSPMOs@CuS NPs+NIR group and YSPMOs(DOX)@CuS group were able to be inhibited to some extent. Most importantly, with relative tumor volumes (V/V_0) of 0.59±0.16, the tumor sizes of the mice were significantly suppressed after treatment with YSPMOs(DOX)@CuS+NPs+NIR.

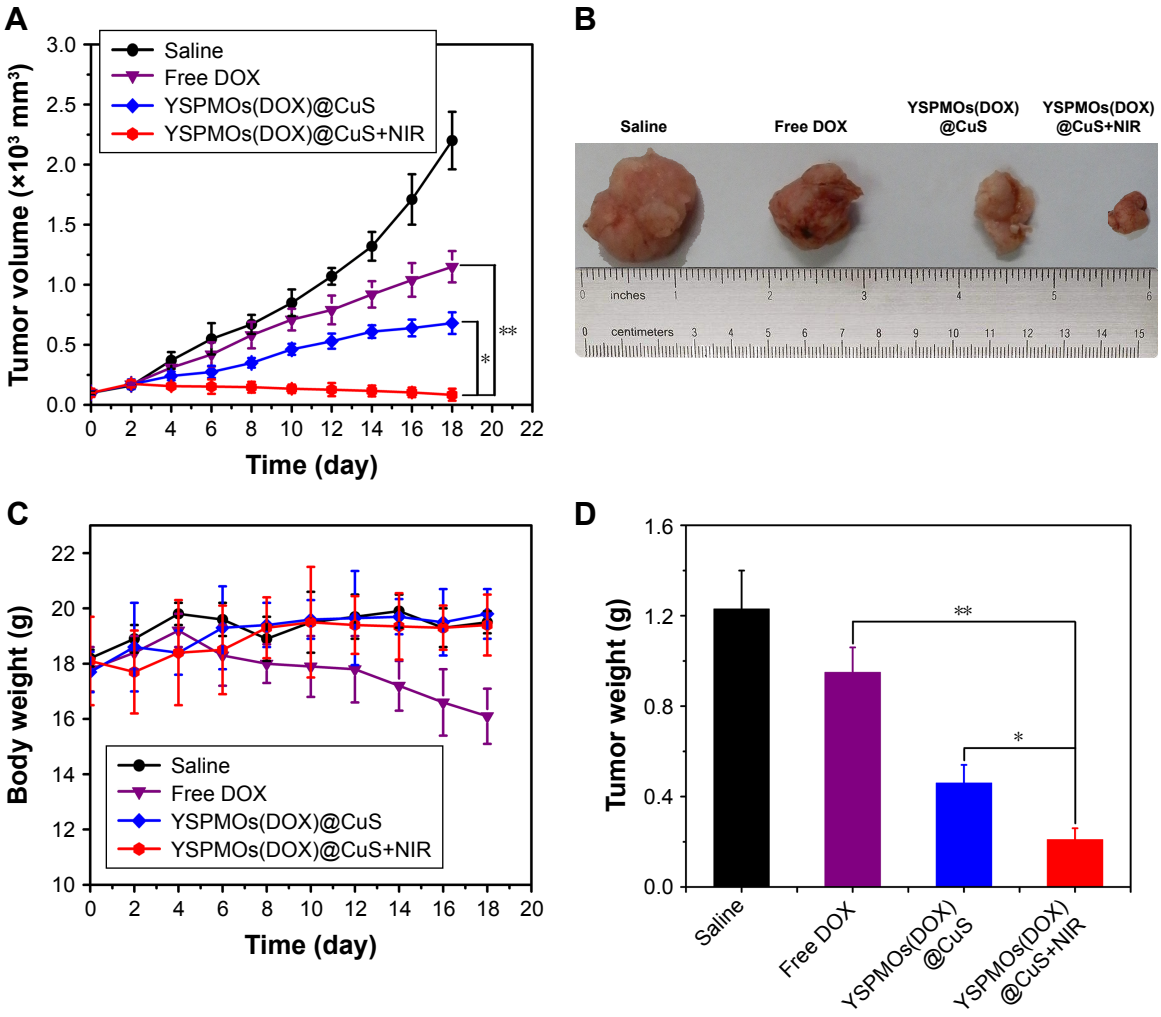

Figure 6 (*Continued*)

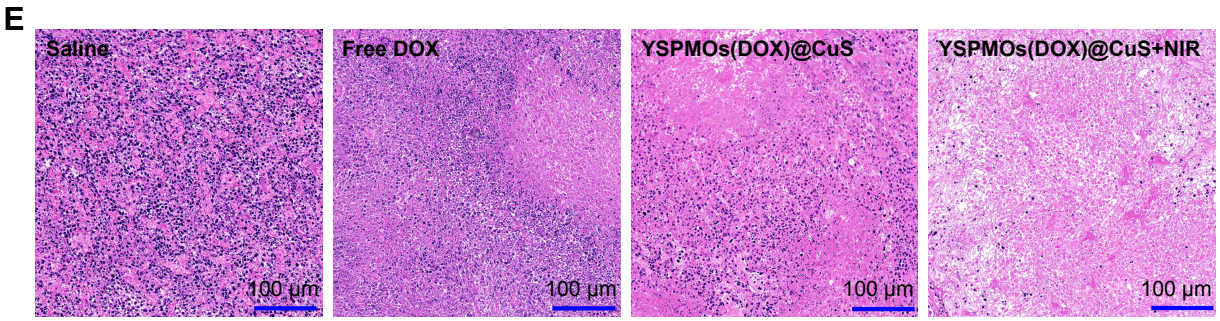

Figure 6 In vivo antitumor activity.
Notes: (**A**) Tumor growth curves of mice after various treatments. (**B**) Photographs of tumor blocks collected from different treatment groups of mice on day 18. (**C**) Body weight changes of mice in different treatment groups within 18 days. (**D**) The tumor weights at the end of therapy on day 18. (**E**) Representative H&E sections of tumors after different treatments. *$p<0.05$, **$p<0.01$.
Abbreviations: H&E, hematoxylin and eosin; YSPMOs, yolk–shell-structured periodic mesoporous organosilica nanoparticles.

The photographs of tumor blocks isolated at day 18 confirmed that the mice treated with YSPMOs(DOX)@CuS in combination with NIR irradiation had the smallest tumor size (Figure 6B). Furthermore, the body weights were recorded during treatment and no obvious change in the mice weight was found in the treatment of YSPMOs(DOX)@CuS plus laser irradiation, indicating the limited toxicity of the NPs (Figure 6C). Here, it should be noted that there was about 10% body weight loss for the mice treated with free DOX, indicating the potential toxicity of free DOX. Furthermore, the average tumor weight is shown in Figure 6D to further illustrate the good antitumor efficacy of YSPMOs(DOX)@CuS plus laser irradiation in vivo.

Afterwards, H&E staining was performed to evaluate the effects of different therapeutic strategies (Figure 6E). Shrinkage of nuclei, nuclear fragmentation, and loss of tumor cells were observed to different extents. As expected, YSPMOs(DOX)@CuS+NIR group displayed significant large-area apoptotic or necrotic regions in tumor tissues. The above results confirmed that the YSPMOs(DOX)@CuS+NIR exhibited the highest antitumor efficiency, mainly due to the synergistic effect of chemotherapy and PTT, with the tendency corresponding to the results of antitumor effect in vitro/vivo. Moreover, for YSPMOs(DOX)@CuS and YSPMOs(DOX)@CuS+NIR, no apparent inflammation, injury, necrosis, and obvious toxicity of the nanosystem were observed in the major organs (heart, liver, spleen, lung, and kidney) according to the results of H&E staining (Figure 7), suggesting the relatively lower systemic toxicity.

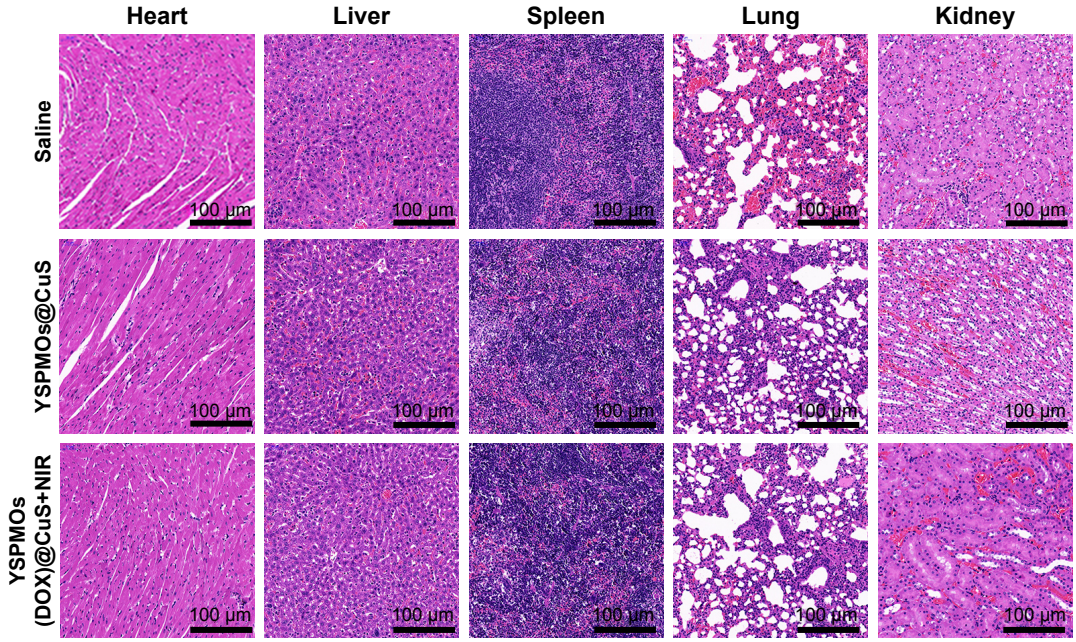

Figure 7 Representative H&E sections of organ tissues (heart, liver, spleen, lung, and kidney) of tumor-bearing BALB/c mice after different treatments.
Abbreviations: H&E, hematoxylin and eosin; NIR, near infrared; YSPMOs, yolk–shell-structured periodic mesoporous organosilica nanoparticles.

In vivo biodistribution

To analyze the in vivo behavior of the YSPMOs(DOX)@CuS more accurately, biodistribution of the nanocarriers was also measured by ICP-OES analysis. As shown in Figure S6, a huge amount of Cu accumulated in the liver and spleen because of the reticuloendothelial system located in these organs.[44] More importantly, the accumulation of the Cu at the tumor site was dramatically increased with time. This indicated that the YSPMOs(DOX)@CuS NPs could be accumulated to the tumor region through a passive enhanced-permeability-and-retention effect.

Conclusion

In summary, we have demonstrated here a multifunctional triple-responsive drug delivery system of YSPMOs(DOX)@CuS for combination chemotherapy and PTT of tumors. The YSPMOs served as a high-payload drug-loading carrier, and CuS, which have NIR laser-induced photothermal conversion efficiency (70.8%), served as a gatekeeper to modified YSPMOs with reduction-cleavable disulfide bond. Considering the low-pH and GSH-rich tumor microenvironment and photothermal effect of CuS, the more precise release of preloaded DOX could be realized through the breakage of the disulfide bond between CuS and YSPMOs in the presence of intracellular GSH. Most importantly, the developed YSPMOs(DOX)@CuS complexes were able to accumulate in tumor sites, and exert combination chemotherapy and PTT of cancer cells in vitro, and a subcutaneous tumor model in vivo, resulting in an outstanding synergistic suppression of tumor growth in the chemo-photothermal therapy. Overall, our study implies that this multifunctional triple-responsive nanoplatform holds great potential for controllable drug release, as well as for combination chemotherapy and PTT of different types of tumors.

Acknowledgments

We greatly appreciate the financial support from the National Natural Science Foundation of China (81772433), the Science and Technology Commission of Shanghai Municipality (16411972200), and the project of Shanghai Municipal Health Bureau (201540100).

Disclosure

The authors report no conflicts of interest in this work.

References

1. Miller KD, Siegel RL, Lin CC, et al. Cancer treatment and survivorship statistics, 2016. *CA Cancer J Clin*. 2016;66(4):271–289.
2. Perez-Herrero E, Fernandez-Medarde A. Advanced targeted therapies in cancer: drug nanocarriers, the future of chemotherapy. *Eur J Pharm Biopharm*. 2015;93:52–79.
3. Lepor H. Surgical treatment of prostate carcinoma. *J Urol*. 2017;197:S41–S42.
4. Topalian SL, Drake CG, Pardoll DM. Immune checkpoint blockade: a common denominator approach to cancer therapy. *Cancer Cell*. 2015;27(4):450–461.
5. Tang Y, McGoron AJ. Combined effects of laser-ICG photothermotherapy and doxorubicin chemotherapy on ovarian cancer cells. *Photochem Photobiol*. 2009;97(3):138–144.
6. Lu N, Huang P, Fan W, et al. Tri-stimuli-responsive biodegradable theranostics for mild hyperthermia enhanced chemotherapy. *Biomaterials*. 2017;126:39–48.
7. Liu J, Wang C, Wang X, et al. Mesoporous silica coated single-walled carbon nanotubes as a multifunctional light-responsive platform for cancer combination therapy. *Adv Funct Mater*. 2015;25(3):384–392.
8. Suteewong T, Sai H, Cohen R, et al. Highly aminated mesoporous silica nanoparticles with cubic pore structure. *J Am Chem Soc*. 2011;133(2):172–175.
9. Jiao J, Liu C, Li X, et al. Fluorescent carbon dot modified mesoporous silica nanocarriers for redox-responsive controlled drug delivery and bioimaging. *J Colloid Interface Sci*. 2016;483:343–352.
10. Hou L, Zhu C, Wu X, Chen G, Tang D. Bioresponsive controlled release from mesoporous silica nanocontainers with glucometer readout. *Chem Commun*. 2014;50(12):1441–1443.
11. Lin CX, Qiao SZ, Yu CZ, Ismadji S, Lu GQ. Periodic mesoporous silica and organosilica with controlled morphologies as carriers for drug release. *Micropor Mesopor Mat*. 2009;117(1–2):213–219.
12. Hu H, Liu J, Yu J, et al. Synthesis of Janus Au@periodic mesoporous organosilica (PMO) nanostructures with precisely controllable morphology: a seed-shape defined growth mechanism. *Nanoscale*. 2017;9(14):4826–4834.
13. Qiao SZ, Yu CZ, Xing W, Hu QH, Djojoputro H, Lu GQ. Synthesis and bio-adsorptive properties of large-pore periodic mesoporous organosilica rods. *Chem Mater*. 2005;17:6172–6176.
14. Croissant JG, Cattoen X, Wong MC, Durand JO, Khashab NM. Syntheses and applications of periodic mesoporous organosilica nanoparticles. *Nanoscale*. 2015;7(24):20318–20334.
15. Liu J, Yang Q, Zhang L, et al. Thioether-bridged mesoporous organosilicas: mesophase transformations induced by the bridged organosilane precursor. *Adv Funct Mater*. 2007;17(4):569–576.
16. Zhang Y, Hou Z, Ge Y, et al. DNA-hybrid-gated photothermal mesoporous silica nanoparticles for NIR-responsive and aptamer-targeted drug delivery. *ACS Appl Mater Interfaces*. 2015;7(37):20696–20706.
17. Lei Q, Qiu WX, Hu JJ, et al. Multifunctional mesoporous silica nanoparticles with thermal-responsive gatekeeper for NIR light-triggered chemo/photothermal therapy. *Small*. 2016;12(31):4286–4298.
18. Wen J, Yang K, Liu F, Li H, Xu Y, Sun S. Diverse gatekeepers for mesoporous silica nanoparticle based drug delivery systems. *Chem Soc Rev*. 2017;46(19):6024–6045.
19. Wu J, Bremner DH, Niu S, et al. Functionalized MoS_2 nanosheet-capped periodic mesoporous organosilicas as a multifunctional platform for synergistic targeted chemo-photothermal therapy. *Chem Eng J*. 2018;342:90–102.
20. Yang S, Chen D, Li N, et al. Hollow Mesoporous silica nanocarriers with multifunctional capping agents for in vivo cancer imaging and therapy. *Small*. 2016;12(3):360–370.
21. Xiao D, Hu JJ, Zhu JY, Wang SB, Zhuo RX, Zhang XZ. A redox-responsive mesoporous silica nanoparticle with a therapeutic peptide shell for tumor targeting synergistic therapy. *Nanoscale*. 2016;8(37):16702–16709.
22. Chen T, Yang N, Fu J. Controlled release of cargo molecules from hollow mesoporous silica nanoparticles based on acid and base dual-responsive cucurbit[7]uril pseudorotaxanes. *Chem Commun*. 2013;49(58):6555–6557.

23. Tang Y, Hu H, Zhang MG, et al. An aptamer-targeting photoresponsive drug delivery system using "off-on" graphene oxide wrapped mesoporous silica nanoparticles. *Nanoscale*. 2015;7(14):6304–6310.
24. Dinggeng H, Xuecai L, Xiaoxiao H, et al. Noncovalent assembly of reduced graphene oxide and alkyl-grafted mesoporous silica: an effective drug carrier for near-infrared light-responsive controlled drug release. *J Mater Chem B*. 2015;3(27):5588–5594.
25. Krishna V, Singh A, Sharma P, et al. Polyhydroxy fullerenes for non-invasive cancer imaging and therapy. *Small*. 2010;6(20):2236–2241.
26. Wang Y, Wang K, Zhao J, et al. Multifunctional mesoporous silica-coated graphene nanosheet used for chemo-photothermal synergistic targeted therapy of glioma. *J Am Chem Soc*. 2013;135(12):4799–4804.
27. Wang T, Guan B, Wang X, et al. Mesostructured TiO_2 gated periodic mesoporous organosilica-based nanotablets for multistimuli-responsive drug release. *Small*. 2015;11(44):5907–5911.
28. Lu N, Tian Y, Tian W, et al. Smart cancer cell targeting imaging and drug delivery system by systematically engineering periodic mesoporous organosilica nanoparticles. *ACS Appl Mater Interfaces*. 2016;8(5):2985–2993.
29. Parambadath S, Mathew A, Jenisha Barnabas M, Ha CS. A pH-responsive drug delivery system based on ethylenediamine bridged periodic mesoporous organosilica. *Micropor Mesopor Mat*. 2015;215:67–75.
30. Yang W, Guo W, Le W, et al. Albumin-bioinspired Gd:CuS nanotheranostic agent for in vivo photoacoustic/magnetic resonance imaging-guided tumor-targeted photothermal therapy. *ACS Nano*. 2016;10(11):10245–10257.
31. Zhou M, Li J, Liang S, Sood AK, Liang D, Li C. CuS nanodots with ultrahigh efficient renal clearance for positron emission tomography imaging and image-guided photothermal therapy. *ACS Nano*. 2015;9(7):7085–7096.
32. Su X, Zhao F, Wang Y, Yan X, Jia S, Du B. CuS as a gatekeeper of mesoporous upconversion nanoparticles-based drug controlled release system for tumor-targeted multimodal imaging and synergetic chemo-thermotherapy. *Nanomed Nanotechnol Biol Med*. 2017;13(5):1761–1772.
33. Wu J, Liu Y, Tang Y, et al. Synergistic chemo-photothermal therapy of breast cancer by mesenchymal stem cell-encapsulated yolk-shell GNR@HPMO-PTX nanospheres. *ACS Appl Mater Interfaces*. 2016;8(28):17927–17935.
34. Feng W, Chen L, Qin M, et al. Flower-like PEGylated MoS_2 nanoflakes for near-infrared photothermal cancer therapy. *Sci Rep*. 2015;5:17422–17435.
35. Li J, Hu Y, Yang J, et al. Hyaluronic acid-modified Fe_3O_4@Au core/shell nanostars for multimodal imaging and photothermal therapy of tumors. *Biomaterials*. 2015;38:10–21.
36. Wu L, Wu M, Zeng Y, et al. Multifunctional PEG modified DOX loaded mesoporous silica nanoparticle@CuS nanohybrids as photo-thermal agent and thermal-triggered drug release vehicle for hepatocellular carcinoma treatment. *Nanotechnology*. 2015;26(2):025102.
37. Teng Z, Su X, Lee B, et al. Yolk–shell structured mesoporous nanoparticles with thioether-bridged organosilica frameworks. *Chem Mater*. 2014;26(20):5980–5987.
38. Ramamoorthy C, Rajendran V. Synthesis and characterization of CuS nanostructures: structural, optical, electrochemical and photocatalytic activity by the hydro/solvothermal process. *Int J Hydrogen Energy*. 2017;42:26454–26463.
39. Zhao B, Gao S, Fan B, Zhao W, Xie Y, Zhang R. Synthesis of flower-like CuS hollow microspheres based on nanoflakes self-assembly and their microwave absorption properties. *J Mater Chem A*. 2015;3:10345–10352.
40. Yang Y, Aw J, Xing B. Nanostructures for NIR light-controlled therapies. *Nanoscale*. 2017;9(11):3698–3718.
41. Luo Z, Hu Y, Cai K, et al. Intracellular redox-activated anticancer drug delivery by functionalized hollow mesoporous silica nanoreservoirs with tumor specificity. *Biomaterials*. 2014;35:7951–7962.
42. Hauck TS, Jennings TL, Yatsenko T, Kumaradas JC, Chan WCW. Enhancing the toxicity of cancer chemotherapeutics with gold nanorod hyperthermia. *Adv Mater*. 2008;20:3832–3838.
43. Jaque D, Martinez Maestro L, del Rosal B, et al. Nanoparticles for photothermal therapies. *Nanoscale*. 2014;6:9494–9530.
44. Gao D, Sheng Z, Liu Y, et al. Protein-modified CuS nanotriangles: a potential multimodal nanoplatform for in vivo tumor photoacoustic/magnetic resonance dual-modal imaging. *Adv Healthcare Mater*. 2017;6(1):1601094–1601105.

Supplementary materials

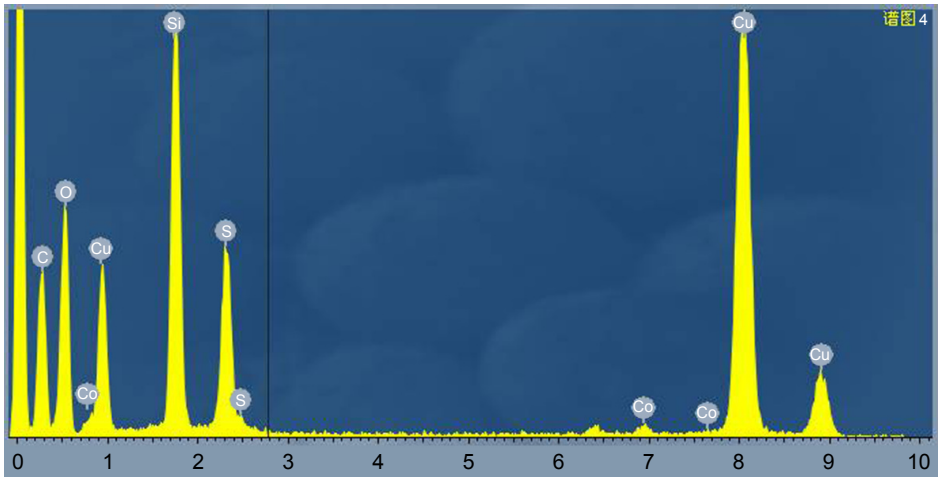

Figure S1 EDX element analysis of YSPMOs(DOX)@CuS.
Abbreviations: DOX, doxorubicin; EDX, energy-dispersive spectra; YSPMOs, yolk–shell-structured periodic mesoporous organosilica nanoparticles.

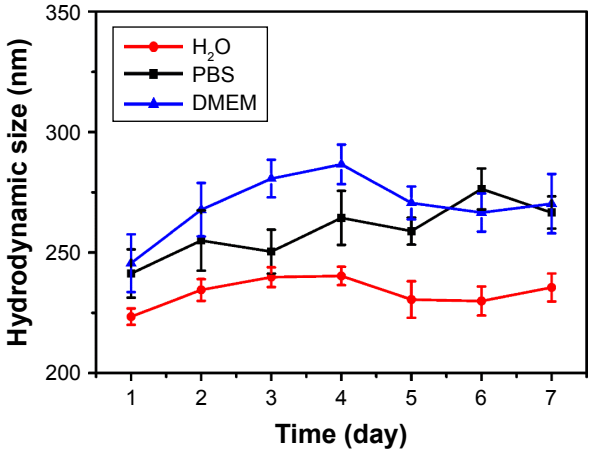

Figure S2 Hydrodynamic size of YSPMOs(DOX)@CuS nanoparticles dispersed in different solutions for 7 days.
Abbreviations: DOX, doxorubicin; YSPMOs, yolk–shell-structured periodic mesoporous organosilica nanoparticles.

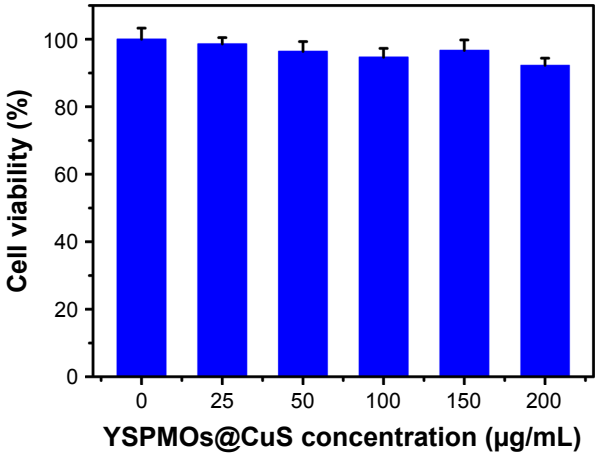

Figure S3 Cell viability of MDA-MB-231 cells incubated with blank YSPMOs@CuS nanoparticles.
Abbreviation: YSPMOs, yolk–shell-structured periodic mesoporous organosilica nanoparticles.

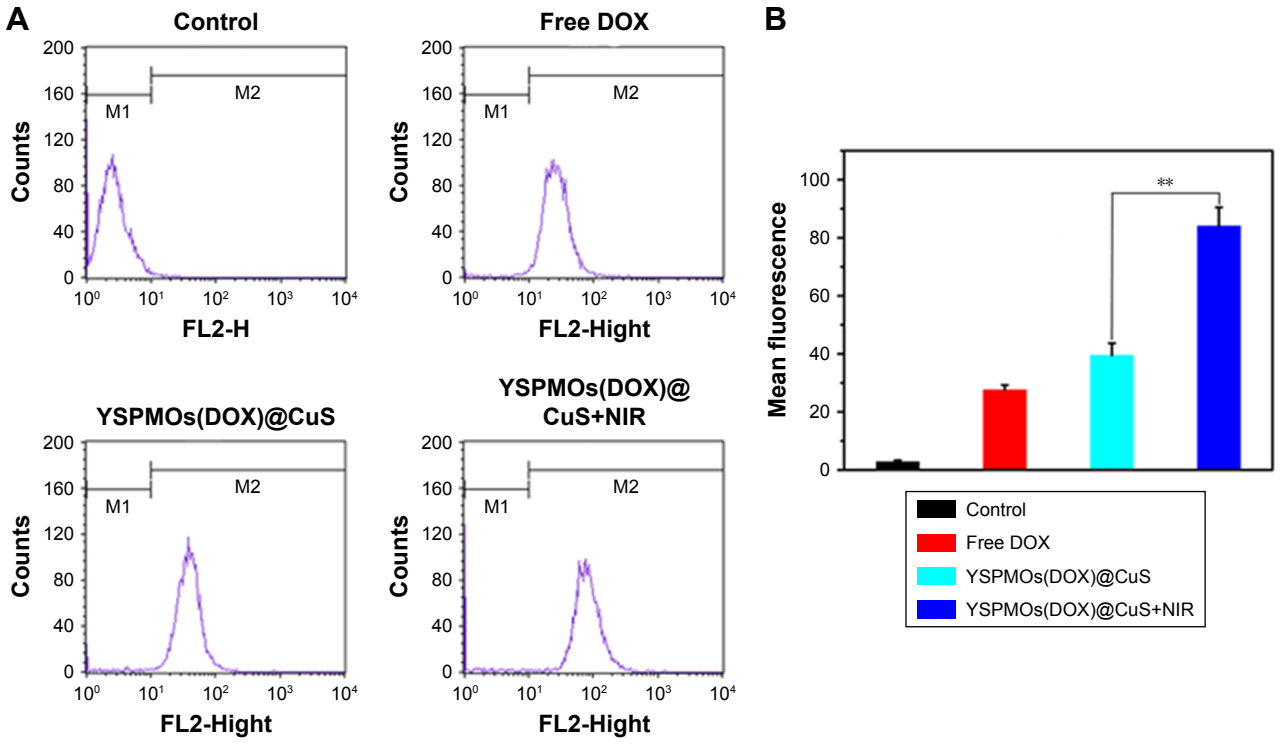

Figure S4 (**A**) Flow cytometry analysis of MDA-MB-231 cells incubated with free DOX and YSPMOs(DOX)@CuS nanoparticles with or without NIR irradiation. (**B**) Fluorescence intensity of MDA-MB-231 cells incubated with free DOX and YSPMOs(DOX)@CuS nanoparticles with or without NIR irradiation. $^{**}P<0.01$.
Abbreviations: DOX, doxorubicin; NIR, near infrared; YSPMOs, yolk–shell-structured periodic mesoporous organosilica nanoparticles.

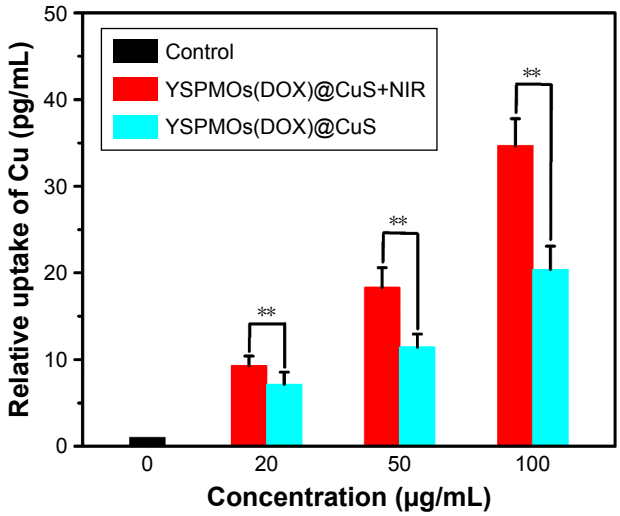

Figure S5 Relative Cu uptake in MDA-MB-231 cells treated with the YSPMOs(DOX)@CuS with or without NIR irradiation at different concentrations for 6 h.
Note: $^{**}P<0.01$.
Abbreviations: DOX, doxorubicin; NIR, near infrared; YSPMOs, yolk–shell-structured periodic mesoporous organosilica nanoparticles.

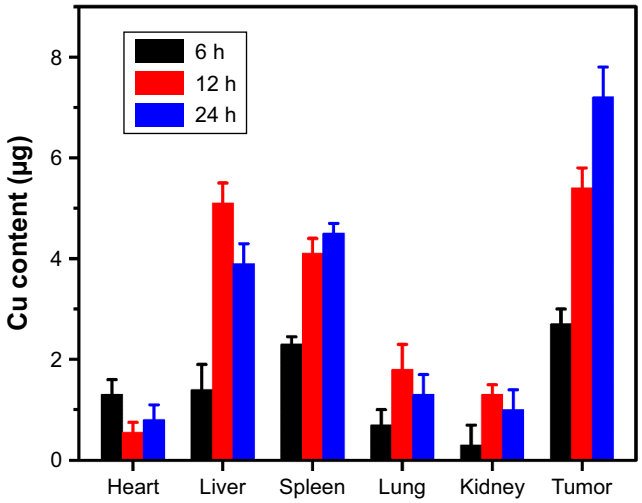

Figure S6 In vivo biodistribution of Cu element in different organs and tumor at different time points post-intravenous injection of the YSPMOs(DOX)@CuS.
Abbreviations: DOX, doxorubicin; YSPMOs, yolk–shell-structured periodic mesoporous organosilica nanoparticles.